Cover Page

1) Title of the paper:

Vascular Models (VaMos): Application to bifurcation classification and aneurysm detection

2) authors' affiliation and address:

LTeN, UMR-6607, Polytech' Nantes, France

&

INSERM, UMR-1087, l'institut du thorax, Nantes, France.

3) e_mail address:

Florent.Autrusseau@univ-nantes.fr

4) Conference & Publisher information:

https://icpr2024.org/

5) bibtex entry:

```
@InProceedings{ICPR2024_VaMos,
  author    = {R. Nader and V. {L'Allinec} and R. Bourcier and F. Autrusseau},
  title     = {Vascular Models (VaMos): Application to bifurcation classification and
               aneurysm detection},
  booktitle = {International Conference on Pattern Recognition (ICPR)},
  year      = {2024},
  date      = {2024-12-01},
  address = {Kolkata, India}
}
```

Synthetic Vascular Models : Application to bifurcation classification and aneurysm detection*

Rafic Nader[1][0000−0001−9493−9980], Vincent L'Allinec[2][0000−0001−8146−5886], Romain Bourcier[1,3][0000−0002−6506−4019], and Florent Autrusseau[1,4][0000−0002−2690−0029]

[1] Nantes Université, CHU Nantes, CNRS, INSERM, l'institut du thorax, F-44000 Nantes, France
[2] CHU Angers, neuro-radiology department, Angers, France
[3] CHU Nantes, neuro-radiology department, Nantes, France
[4] Ecole Polytechnique de l'Université de Nantes, LTeN, U6607, Nantes Université, Nantes, France
Florent.Autrusseau@univ-nantes.fr

Abstract. In this work, we present new synthetic vascular models that tries to mimic various portions of the cerebral vascular tree, as acquired from Magnetic Resonance Angiography - Time of Flight modality - acquisitions. Not only are these vascular models able to replicate the cerebral arteries, but also, the bifurcations formed by the arteries, and furthermore, one option within the models allows to embed an intracranial aneurysm. Our goal in designing this set of tools was to train convolutional neural networks for various pattern recognition tasks; namely, we intend to label the main bifurcations forming the Circle of Willis, or to automatically detect intracranial aneurysms. However, to efficiently train a neural network, the fidelity of the mimicked vascular portions is of paramount importance.

Keywords: Cerebral vascular tree · Cerebral bifurcations · Circle of Willis · synthetic model · intracranial aneurysms .

1 Introduction

Various diseases may occur along the vascular tree. Such accidents can be particularly critical when located within the brain. Among the various vascular pathologies, the intracranial aneurysms (ICA) can be particularly devastating [16]. Cerebral aneurysms commonly occur onto the bifurcations forming a central arterial structure named the Circle of Willis (CoW) [3]. More specifically, they arise between the daughter arteries, they are referred to as saccular aneurysms, due to their balloon shape. Intracranial aneurysms occur for 3 to 5% of the world population.

* This work was supported by projects "eCAN" #ANR-23-RHUS-0013, #ANR-21-CE17-0006 and INSERM CoPoC #MAT-PI-22155-A-01

While an aneurysm itself may not pose immediate harm, if it bleeds (ruptures), it induces severe consequences such as subarachnoid hemorrhage, resulting in death (35%) or serious cognitive deficits (46%) [13]. Hence, it is crucial to not only, automatically detect the aneurysms, but also, to monitor the portions of the CoW presenting a higher risk (see Fig. 1). Prior to the emergence of deep learning techniques such as Convolutional Neural Networks (CNNs), fewer works focused on probabilistic or traditional machine learning approaches for labeling the Circle of Willis bifurcations [2, 17, 21]. Recent advances include a deep learning based method for CoW arteries segmentation [7] and a two-step pipeline for detecting CoW vascular bifurcations [14]. In the context of aneurysms detection, various deep learning-based methods have emerged for the segmentation and/or detection of ICAs [9, 15, 18]. Of particular interest, the ADAM Challenge [20] compared 11 distinct deep learning approaches aimed at detecting and/or segmenting aneurysms. It is crucial to highlight that the majority of existing methods have been developed using private clinical data, which includes meticulously refined manual annotations. Indeed, when it comes to artificial intelligence, there is a recurring burden : the acquisition of manual annotation. To address this issue, the authors in [6] suggested employing "weak" annotations.

In this work, we intend to propose some alternatives to these manual annotations. We have designed a set of synthetic Vascular Models (VaMos) [5] which purpose is specifically to train CNNs. Although one can find synthetic models in the literature, the final aim differs. In [10], the authors used Constrained Constructive Optimization (CCO) for arterial model tree generation, mainly focusing on predicting vascular network growth. Similarly, works in [19] proposed a macroscopic model emphasizing angiogenesis and capillary sprout formation, and authors in [11] exploited CCO to estimate liver vascular network growth. The work in [4] used CCO onto cerebral arteries, and incorporated level set functions for growth estimation. Later, authors in [8, 22] proposed *VascuSynth*, a numerical vascular tree generation tool intended to model not only the geometrical layout of the arterial tree, but also simulating the background noise, albeit with limited accuracy in replicating the artery tortuosity. More recently, SimVascular [12] offered advanced 3D mesh modeling for cardiovascular simulation but lacks flexibility in modifying the geometry or modeling background noise. Unfortunately, none of these models could be efficiently exploited along with machine learning methods for Computer-Aided Diagnosis. Another interesting approach was proposed in [5] where the authors generate synthetic blood vessels surfaces. Variational Autoencoders and Generative Adversarial Networks were used to generate mesh like 3D arteries and try to model stenosis; but only onto isolated arteries, neither bifurcations, nor aneurysms were considered.

In this paper, we aim to come up with a highly reliable synthetic vascular model. We aim to generate a substantial (synthetic) image dataset to train various Deep-Learning algorithms. The rationale behind our approach is to demonstrate that, even with a small dataset, if supplemented by VaMos, we can achieve excellent results. In Section 2, we will present VaMos in details. In Section 3, we

[5] Available here : https://gitlab.univ-nantes.fr/autrusseau-f/vamos

will evaluate the improvements brought by the synthetic data on two distinct tasks: *i)* bifurcations classification, and *ii)* ICA detection. Finally, in Section 4, we conclude our work by summarizing the key findings.

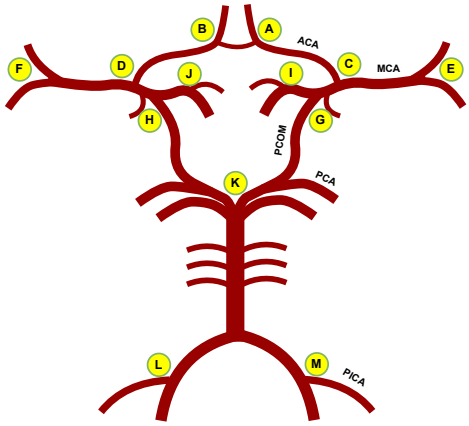

Fig. 1: Bifurcations of Interest along the Circle of Willis (Yellow tags)

2 VaMos : Vasculature Models

Fig. 2 shows the overall structure of the Vasculature Models. Overall, three important vascular components are being modeled : the arteries, the bifurcations and the aneurysms. This means, one could either generate synthetic branches for segmentation purpose, or bifurcations for their classification, or, it would also be possible to generate only synthetic ICA to be merged onto actual MRI images for their detection. Moreover, besides the different geometrical shapes of the vascular tree, the various background matters are also mimicked (gray/ white matters, cerebro-spinal fluid, lateral ventricles, etc.). The upper part in Fig. 2 (yellow shaded block) represents the background noise modeling, whereas the lower part (light blue shaded block), shows the replication of the arterial geometry. In order to generate synthetic images with adjustable resemblance to the ground truth, the VaMos have been designed to modify everything from its basis image portion. Indeed the five green ellipses show all the modifications that can be brought onto an aneurysm bearing bifurcation; namely, we can *i)* tweak the background shape, *ii)* modulate the noise amplitudes, *iii)* adjust the arteries' tortuosity, *iv)* change the diameters, and finally, *v)* add up an ICA (while modifying its shape). So far, our model has been designed, adjusted and tested on Magnetic Resonance Angiography images, with Time-of-Flight modalities (MRA-TOFs).

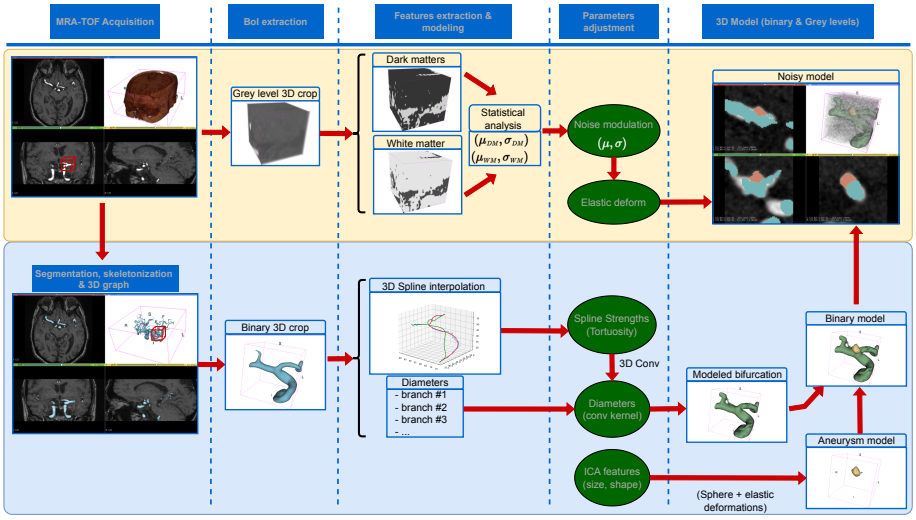

Fig. 2: Structure of the synthetic Vasculature Models.

2.1 Modeling the structure of the bifurcations

From the binary representation of a given MRA-TOF acquisition, the 3D skeleton is first computed, and then, the 3D graph is collected. Each single branch from a given cropped area of interest (typically located around a bifurcation of the CoW) is identified, the voxels along the centerline are represented as a 3D curve, on which 3D B-splines will be fitted. Each branch (artery) can thus be represented by the knots, the B-spline coefficients and the degree of the spline. It is then relatively easy to tweak the 3D spline model by modifying details on B-spline equations fitting. Figure 3 represents two different spline coefficients modifications for a given bifurcation. The blue lines represent the actual bifurcation centerline, the red lines represents the best 3D fit, whereas the green lines stand for the modified 3D splines (left panel : weak modifications and right panel: stronger variation of the 3D splines).

2.2 Modeling the background gray levels

In the aim to generate a 3D noise presenting strong similarities with our target MRA-TOF, our approach consists in producing a higher frequency noise patch, which will be subsequently filtered through a predefined filter kernel, so as to reach the target statistical properties. In other words, if a Gaussian noise patch of standard deviation σ_0 goes through a Gaussian filter of standard deviation σ_f, the resulting filtered noise will present a standard deviation σ_G, such that:

$$\sigma_G \approx \frac{\sigma_0}{(2\sigma_f\sqrt{\pi})} \tag{1}$$

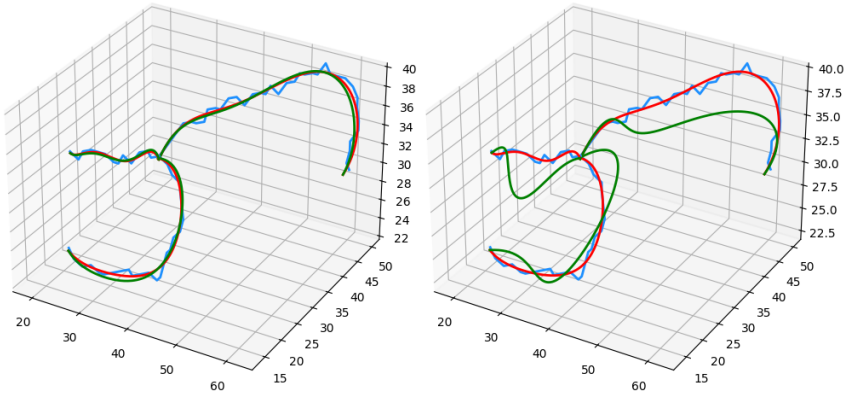

Fig. 3: 3D spline fit of the three arteries forming a bifurcation for two distinct spline modification parameters.

Indeed, when an image, composed of Gaussian noise of standard deviation σ_0 is being filtered by a Gaussian filter of standard deviation σ_G, the so-obtained filtered image ends up with a standard deviation of σ_f. according to the eq. 8. For our particular purpose, we intend to determine which Gaussian filter (of standard deviation σ_G) shall be used on the input image so as to obtain a filtered image with a given target statistics (σ_f), and hence $\sigma_G \approx \sigma_0/(2\sigma_f\sqrt{\pi})$.

This allows us to generate a high frequency noise of average set to our target 3D crop. This noise will then be smoothed by a Gaussian filter (σ_G). The resulting image (of standard deviation σ_f) will thus present strong statistical similarities with the target portion of the MRA-TOF being modeled. Evidently, our model allows to target slightly different statistical noises as the one extracted from the ground truth cropped area.

An input image $I(x, y)$ is Gaussian filtered as :

$$O(x,y) = \sum_{i=-\infty}^{\infty} \sum_{j=-\infty}^{\infty} \frac{1}{2\pi\sigma_G^2} e^{-\frac{i^2+j^2}{2\sigma_G^2}} I(x+i, y+j) \tag{2}$$

According to the Bienaymé's identity :

$$Var\left(\sum_{i=1}^{n} X_i\right) = \sum_{i=1}^{n} Var(X_i) + \sum_{i,j=1,i\neq j}^{n} Cov(X_i, X_j) \tag{3}$$

And thus, the variance is:

$$Var\left(\sum_{i=1}^{n} c_i X_i\right) = \sum_{i=1}^{n} c_i^2 Var(X_i) + 2 \times \sum_{i,j=1,i\neq j}^{n} c_i c_j Cov(X_i, X_j) \tag{4}$$

However, if $X_i, ..., X_n$ are pairwise independent ($Cov(X_i, X_j) = 0$, $\forall (i \neq j)$):

$$Var\left(\sum_i c_i X_i\right) = \sum_i c_i^2 Var(X_i) \tag{5}$$

(c_i being constants). We consider that the variance of $I(x,y)$ is $Var\left[I(x+i,y+i)\right] = \sigma_0^2$; we estimate the variance of the output image $Var\left[O(x,y)\right] = \sigma_f^2$. Thus,

$$\sigma_f^2 = \sigma_0^2 \sum_{j=-\infty}^{\infty} \sum_{i=-\infty}^{\infty} \left(\frac{1}{2\pi\sigma_G^2} e^{-\frac{i^2+j^2}{2\sigma_G^2}} \right)^2 \tag{6}$$

For large σ_G, the sum can be approximated as:

$$\begin{aligned} \sigma_f^2 &\approx \sigma_0^2 \int_{-\infty}^{\infty} \int_{-\infty}^{\infty} \left(\frac{1}{2\pi\sigma_G^2} e^{-\frac{i^2+j^2}{2\sigma_G^2}} \right)^2 di.dj \\ &= \frac{\sigma_0^2}{4\pi\sigma_G^2} \end{aligned} \tag{7}$$

and thus,

$$\sigma_f \approx \frac{\sigma_0}{2\sigma_G\sqrt{\pi}} \tag{8}$$

2.3 Adding an intracranial aneurysm

Besides the generation of highly similar and yet easily tunable arteries, our models allow to embed an intracranial saccular aneurysm between the daughter arteries. The ICA is located onto the bisector of the two daughter arteries, at a distance $\mathcal{D}$ from the bifurcation center such that:

$$\mathcal{D} = r \times \gamma + \sqrt{\left(\frac{R}{tan(\Theta/2)} \right)^2 + R^2} \tag{9}$$

R being the average artery radius, Θ the angle between the daughter arteries, r is the ICA radius, and γ, a growth factor allowing to push/pull the aneurysm inward/outward the bifurcation.

Figure 4 shows a possible configuration of a bifurcation bearing an aneurysm. The distance $\mathcal{D}$ separating the aneurysm center and the bifurcation node can be computed as shown in the equation (9). The various constituents of this formula are represented in Fig.4.

2.4 Synthetic Model Evaluation

We have conducted a thorough evaluation of the model features in terms of both bifurcation anatomical evaluation, and aneurysm shape. We present on Fig. 5 a comparison between the Ground Truth (GT) bifurcations and those generated by the Synthetic Model (SM). We hereby compare the angles formed by the three arteries, their diameters, as well as their tortuosity.

We can observe that the modeled branches exhibit strong similarities with their respective ground truths. For this comparison experiment, 100 cropped portions of the bifurcation #C (see Fig.1) were evaluated. Similarly, we have evaluated various geometrical properties of the aneurysmal sacs, namely, the

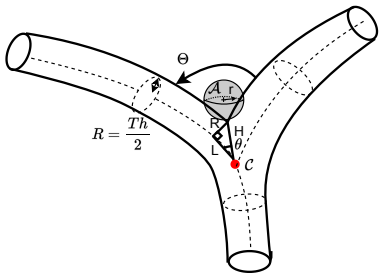

Fig. 4: Position of the synthetic aneurysm along the bisector between the daughter arteries.

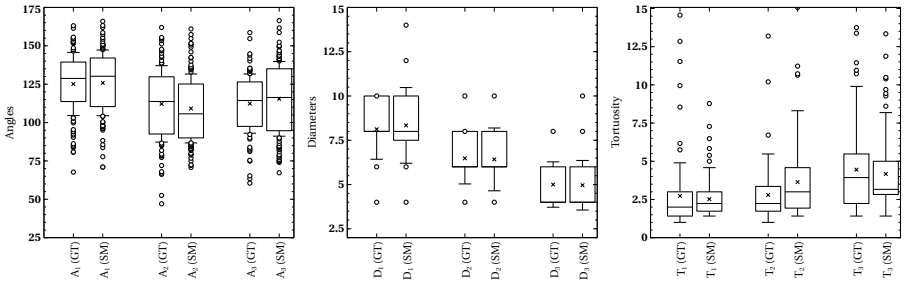

Fig. 5: Evaluation of the bifurcation model with respect to the angles (A), the diameters (D) and branches tortuosity (T).

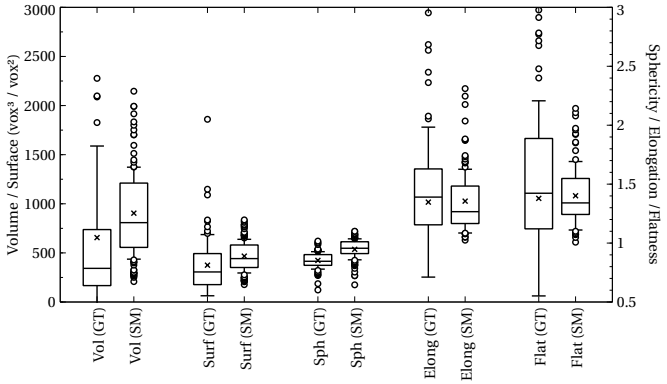

Fig. 6: Evaluation of the modeled aneurysms in terms of sac volume (Vol), outer surface (Surf), Sphericity (Sph), Elongation (Elong) and Flatness(Flat).

ICA volume, the outer surface, as well as the sphericity, elongation and flatness coefficients.

We show on Fig. 6 how the various features of the modeled aneurysm actually match quite accurately the ground truth features. Indeed, we can notice the strong similarities between the MRA-TOF and the modeled features. We can expect the model to be efficiently used to train neural networks. The next section is dedicated to the experimental results.

3 Experiments and results

Let us now present the increased performances brought by using VaMos along with neural networks on two specific tasks: CoW bifurcations classification (Task 1) and aneurysms detection (Task 2) on MRA-TOFs. We demonstrate the efficiency of using the synthetic model alone or as a form of data augmentation for a small dataset.

For each experiment, the images were manually labeled by a trained operator, and validated by an expert neuro-radiologist. The MRI images used in the experiments were collected from different French institutions and were acquired using 19 different MRI scanners from Siemens Healthcare, GE Medical systems, Philips Medical systems and Fujifilm (see Table 1).

Table 1: Summary of the Time of flight (TOF) magnetic resonance imaging (MRI) dataset used in the study.

Dataset	**Maker**	**MR device**	**MFS (T)**
Set-1	GE	Optima MR450W	1.5
Set-2	GE	Optima MR360W	1.5
Set-3	GE	Discovery MR750W	3.0
Set-4	GE	Signa HDxt	1.5
Set-5	GE	Signa HDxt	3.0
Set-6	GE	Signa Artist	1.5
Set-7	SIEMENS	Aera	1.5
Set-8	SIEMENS	Skyra	3.0
Set-9	SIEMENS	Avanto	1.5
Set-10	SIEMENS	Prisma	3.0
Set-11	SIEMENS	Sonata	1.5
Set-12	SIEMENS	Verio	3.0
Set-13	SIEMENS	Magnetom Sola	1.5
Set-14	SIEMENS	Magnetom Amira	1.5
Set-15	Philips	Ingenia	3.0
Set-16	Philips	Ingenia Edition X	3.0
Set-17	Philips	Achieva	3.0
Set-18	Philips	Achieva	1.5
Set-19	Fujifilm	Echelon Oval	3.0

3.1 Task 1: Classification of CoW bifurcations

This section is devoted to the classification of 3D patches encompassing the Bifurcations of Interest (BoI) along the CoW via 3D CNNs. In our research, we focused on the 13 BoI being associated with the highest risk of aneurysm occurrence [17]. These specific bifurcations are depicted in Fig. 1.

Dataset: For Task 1, we have selected 154 MRA-TOF images. For the training phase, a total of 110 images were used, while an independent test dataset was composed of 44 images. To ensure consistency in image dimensions and voxel spacing across the dataset, we re-sampled all MRA-TOFs to a uniform voxel spacing of 0.4 mm^3.

Data annotation and data generation: To annotate the Ground Truth patches, we used a 3D skeleton computed on the vessel segmentation, along with its corresponding 3D undirected graph. The graph nodes help us identifying the center of each bifurcation and extract $32 \times 32 \times 32$ voxel patches with an isotropic voxel size of 0.4 mm around these coordinates, resulting in a total of 1180 bifurcations in the training set and 386 in the test set. To assess the potential enhancements brought by VaMos, we have generated 40 synthetic models for each BoI. These models were designed to replicate the features of the actual bifurcations, with slight modifications (diameters, tortuosity, etc.)

Neural network and evaluation protocol: Building upon our previous research [14], we employed a 3D-CNN for classification purposes (see Fig. 7). The model is composed of nine convolutional layers, each with a kernel size of 3 and a stride of 1. These layers are organized into five convolutional blocks with 32, 64, 128, 256, 512 respective feature channels. The last 3 layers are fully connected. Dropout layer is used for regularization. We implemented the neural networks considered in this work using Tensorflow framework (2.9.0).Training and inference were performed on an NVIDIA RTX A5000 GPU with 16 GB of memory.

We have evaluated the improvements using three different training dataset sizes: D1 (48 TOFs), D2 (82 TOFs), and D3 (110 TOFs). Each dataset was exploited in two distinct experiments: Exp. #B1 involved training exclusively with actual TOF patches, while Exp. #B2 used only synthetic patches for training. Each dataset was partitioned into five folds for cross-validation. The models were trained using categorical cross-entropy loss, Adam optimizer and a learning rate of 0.0001. Training was conducted for 100 epochs, selectively saving the model with the best performance on the validation fold. After training, model evaluation involved using a holdout test set, with final predictions derived by averaging predictions from the five-fold models.

Classification results: Our evaluation aimed to assess the impact of using VaMos across various training dataset sizes. The overall performance is evaluated

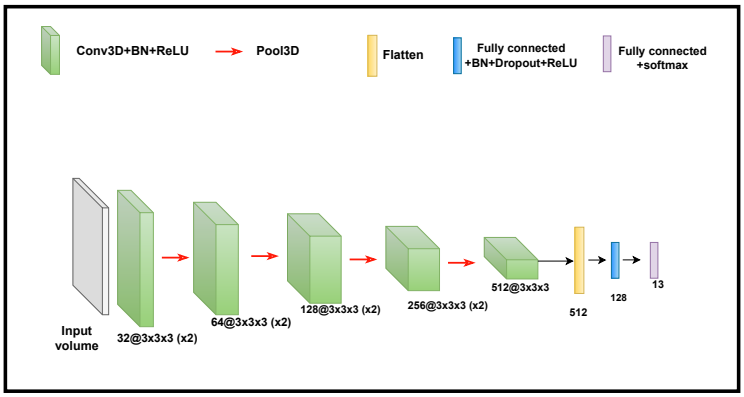

Fig. 7: CNN architecture used for BoIs classification

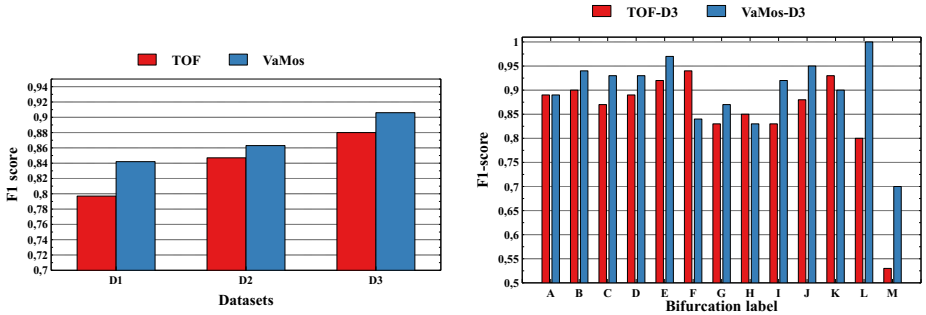

(a) F1-score using different training sets. (b) F1-score by class using dataset D3.

Fig. 8: F1-Score improvements brought by using the VaMos synthetic patches (on the test set).

by computing the F1-score across all the samples for each experiment. The results are shown in Fig. 8a. When using actual TOF patches, we notice a notable increase of F1-score, from 79.7% to 88% when the dataset size increases (from D1 to D3). Similarly, when using VaMos, the F1-scores also significantly increase, from 84.2% to 90.6%, although the degree of variation between cases is less pronounced. Across all datasets, the performances are consistently increased when using VaMos. The improvements are more pronounced for D1 (up to 4.5%) than D2 and D3 (up to 2%). We also report the score for each class (bifurcation label) when using D3 in Figure 8b. We observe on this plot that when VaMos patches are included (blue bars, labeled "VaMos-D3"), a better F1-score is achieved for 9 of the 13 classes, compared to a training using only TOF crops (red bars labeled "TOF-D3").

3.2 Task 2: Aneurysms detection

Let us now evaluate the possible improvements brought by using VaMos in an intracranial aneurysms detection scenario.

Dataset: For Task 2, we have collected 105 scans with unruptured ICAs (distinct from those used in Task 1). The dataset was split into 70 training images, used for both training and validation, and a separate test set of 35 images. Each image contains from 1 to 4 aneurysms, totaling 138 aneurysms with a mean radius of 2.57 ± 0.89 mm.

Data sampling and generation: To address the ICA detection task, we adopted a 3D U-Net implementation used in [6]. This latter was chosen to effectively perform the aneurysm segmentation and its subsequent detection. We use small patches ($64 \times 64 \times 64$ voxels, *i.e.* 25.6 mm wide). For positive samples (with ICA), we extract 10 copies for each aneurysm by shifting its position within the patch. For negative patches, we extract 20 samples for each volume, selected to encompass cerebral arteries (but aneurysm-free). For data generation, 134 aneurysm-free patches from Task 1 served as a basis to generate 998 synthetic patches containing an ICA. Various aneurysms shapes and sizes were simulated by manipulating the radius parameter and applying elastic deformations that emulate the characteristics of original scans, as shown in Fig 6. Moreover for a complete comparison, we apply traditional data augmentation techniques on positive patches, namely rotations within the interval $[-15°, +15°]$ and $(90°, 180°, 270°)$, as well as horizontal and vertical flipping and Gaussian noise addition.

Training and evaluation protocol: The U-Net was optimized using a loss function combining Dice loss and binary Cross-entropy loss along with Adam optimizer and a learning rate of 0.0001. To assess potential improvements brought by VaMos, three distinct experiments were conducted. In Exp. #A1, we trained a baseline model using 50 TOFs (630 positive patches). In Exp. #A2, the training dataset was augmented with patches via 7 traditional data augmentation operations (with a total of 5040 patches ($630 + 7 \times 630$). In Exp. #A3, the training dataset was augmented with the 998 VaMos patches (total of 1628 positive patches). We used the remaining 20 TOFs as a validation data for all three experiments and the separate test set composed of 35 TOFs (with a total of 50 aneurysms) for inference. During the inference stage, patches centered around cerebral bifurcations, identified through an automated vessel segmentation [14] and subsequent 3D undirected graph generation, are selectively retained to target regions most susceptible to aneurysm development, enhancing the accuracy of the results.

ICA detection performance: The performances were assessed on the test set using two key metrics: lesion-level sensitivity and False Positive (FP) rate

(FP per TOF), as outlined in [1]. To calculate the evaluation metrics, each predicted connected component (CC) is treated as a potential detection. If the center of gravity of a CC is present in a ground truth CC, it is classified as a true positive detection. Otherwise, it is labeled as a false positive. In Exp. #A1,

Table 2: The results of aneurysm detection task.

Methods	Sensitivity (%)	FPs/case
Exp. #A1	72	0.37
Exp. #A2	76	1.31
Exp. #A3	88	1.45

the CNN successfully detected 36 aneurysms within a dataset comprising 50 instances, resulting in a lesion-level sensitivity of 72%. This sensitivity increased to 76% in Exp. #A2 with 38 correctly detected aneurysms. However, when incorporating VaMos patches, the lesion level sensitivity reaches 88% with 44 detected aneurysms. Moreover, within Exp. #A1, the network displayed a low false-positive rate of 0.37, which respectively increased to 1.31 and 1.45 for Exp #A2 and Exp #A3 upon incorporating data augmentation (see Table 2).

4 Discussion and Conclusion

In this section, we delve into the impact of the synthetic vasculature model, which effectively mimics portions of MRA-TOF images. The synthetic model encompasses several processes, it accurately models the geometry of cerebral arteries and their bifurcations, it introduces surrounding noise, and incorporates aneurysms of diverse sizes and shapes. Our goal is to provide a comprehensive dataset that can enhance the performance of various deep learning tasks, such as the classification of bifurcations forming the Circle of Willis or the detection of cerebral aneurysms. In this study, we deliberately opted to employ basic deep learning architecture with straightforward optimization techniques. Our primary focus was on the contribution brought by VaMos.

Regarding Task 1, we chose to exclusively use VaMos as the source of training patches. A direct comparison was made with a training solely performed on actual TOF patches. The primary finding is that using hundreds of synthetic patches enhances the classification accuracy across all dataset sizes. This improvement is particularly notable when considering a small dataset (up to a 4.5% increase in F1-score). On average, achieving similar performance is possible by annotating only 82 TOFs supplemented with VaMos, resulting in comparable F1-score (0.863 for VaMos-D2, 0.88 TOF-D3 and 0.906 for VaMos-D3). Our model demonstrates superior performance across most classes, with exceptions observed for classes M, H, and J. The challenges in modeling M may stem from its complex anatomical structure, potentially resulting in trifurcations or quadrifurcations. Uncertainties encountered by neuroradiologists in annotating

the MCA branch likely contribute to discrepancies in class H, while hypoplastic cases of PCOM arteries present challenges for modeling J. Ongoing works focus on adapting VaMos to address these specific cases.

A prominent achievement of our research is the successful generation of synthetic aneurysms seamlessly integrated into MRA scans lacking aneurysms, significantly enriching limited dataset. The primary outcome of Task 2 reveals that training the CNN using VaMos patches as Data augmentation yielded a marked improvement in sensitivity for detecting intracranial aneurysms compared to training solely on actual TOFs. Whereas the latter missed 28% of lesions in the test data, for the former, the CNN only missed 12% aneurysms. Traditional data augmentation techniques yielded only a modest improvement in sensitivity (4%) compared to VaMos (16%). This is consistent with the limitations inherent in these traditional methods. These techniques primarily enhance the model's ability to generalize from existing examples without fundamentally diversifying the range of anatomical structures represented in the training data as they do not introduce variations in critical features such as aneurysm shape and size, which are essential for effectively training models to recognize a wide variety of aneurysms across different patients. In contrast, advanced generation models like VaMos are designed to create more complex and diverse synthetic examples that include significant variations in aneurysm characteristics. This was accomplished with a slight increase in false positive rate highlighting the efficacy of our approach. Missed detection in Exp. #A3 predominantly stemmed from small aneurysms. Out of the 6 missed aneurysms, 4 had a radius below 1.5 mm. For such aneurysms, these missed detection can also be attributed to the uncertainty in the initial expert labeling. Nonetheless, our forthcoming endeavors will specifically target this subset of aneurysms, by generating more synthetic aneurysms with small radius.

References

1. Adams, W., Laitt, R., Jackson, A.: Time of flight 3d magnetic resonance angiography in the follow-up of coiled cerebral aneurysms. Interv Neuroradiol. **5**(2), 127–37 (1999). https://doi.org/10.1177/159101999900500203
2. Bogunovic, H., Pozo, J.M., Cardenes, R., Roman, L.S., Frangi, A.F.: Anatomical labeling of the circle of willis using maximum a posteriori probability estimation. IEEE Transactions on Medical Imaging **32**(9), 1587–1599 (2013)
3. Brown, R.D., Broderick, J.P.: Unruptured intracranial aneurysms: epidemiology, natural history, management options, and familial screening. The Lancet Neurology **13**(4), 393–404 (2014)
4. Bui, A.V., Manasseh, R., Liffman, K., Šutalo, I.D.: Development of optimized vascular fractal tree models using level set distance function. Medical engineering & physics **32**(7), 790–794 (2010)
5. Danu, M., Nita, C.I., Vizitiu, A., Suciu, C., Itu, L.M.: Deep learning based generation of synthetic blood vessel surfaces. In: 2019 23rd International Conference on System Theory, Control and Computing (ICSTCC). pp. 662–667. IEEE (2019)
6. Di Noto, T., Marie, G., Tourbier, S., Alemán-Gómez, Y., Esteban, O., Saliou, G., Cuadra, M.B., Hagmann, P., Richiardi, J.: Towards automated brain aneurysm

detection in tof-mra: Open data, weak labels, and anatomical knowledge. Neuroinformatics **21**(1), 21–34 (2023)
7. Dumais, F., Caceres, M.P., Janelle, F., Seifeldine, K., Arès-Bruneau, N., Gutierrez, J., Bocti, C., Whittingstall, K.: eicab: A novel deep learning pipeline for circle of willis multiclass segmentation and analysis. NeuroImage **260**, 119425 (2022)
8. Hamarneh, G., Jassi, P.: Vascusynth: Simulating vascular trees for generating volumetric image data with ground truth segmentation and tree analysis. Computerized Medical Imaging and Graphics **34**(8), 605–616 (2010). https://doi.org/10.1016/j.compmedimag.2010.06.002
9. Joo, B., Ahn, S.S., Yoon, P.H., Bae, S., Sohn, B., Lee, Y.E., Bae, J.H., Park, M.S., Choi, H.S., Lee, S.K.: A deep learning algorithm may automate intracranial aneurysm detection on mr angiography with high diagnostic performance. European Radiology **30**, 5785–5793 (2020)
10. Karch, R., Neumann, F., Neumann, M., Schreiner, W.: A three-dimensional model for arterial tree representation, generated by constrained constructive optimization. Computers in Biology and Medicine **29**(1), 19–38 (1999). https://doi.org/https://doi.org/10.1016/S0010-4825(98)00045-6, https://www.sciencedirect.com/science/article/pii/S0010482598000456
11. Kretowski, M., Rolland, Y., Bezy-Wendling, J., Coatrieux, J.L.: Physiologically based modeling of 3-d vascular networks and ct scan angiography. IEEE Transactions on Medical Imaging **22**(2), 248–257 (2003). https://doi.org/10.1109/TMI.2002.808357
12. Lan, H., Updegrove, A., Wilson, N.M., Maher, G.D., Shadden, S.C., Marsden, A.L.: A re-engineered software interface and workflow for the open-source simvascular cardiovascular modeling package. Journal of biomechanical engineering **140**(2), 024501 (2018)
13. Ma, N., Feng, X., Wu, Z., Wang, D., Liu, A.: Cognitive impairments and risk factors after ruptured anterior communicating artery aneurysm treatment in low-grade patients without severe complications: A multicenter retrospective study. Front Neurol **12:613785** (2021)
14. Nader, R., Bourcier, R., Autrusseau, F.: Using deep learning for an automatic detection and classification of the vascular bifurcations along the circle of willis. Medical Image Analysis p. 102919 (2023). https://doi.org/https://doi.org/10.1016/j.media.2023.102919, https://www.sciencedirect.com/science/article/pii/S1361841523001792
15. Park, A., Chute, C., Rajpurkar, P., Lou, J., Ball, R.L., Shpanskaya, K.S., Jabarkheel, R., Kim, L.H., McKenna, E., Tseng, J., Ni, J.C., Wishah, F., Wittber, F., Hong, D.S., Wilson, T.J., Halabi, S.S., Basu, S., Patel, B.N., Lungren, M.P., Ng, A., Yeom, K.W.: Deep learning–assisted diagnosis of cerebral aneurysms using the headxnet model. JAMA Network Open **2** (2019), https://api.semanticscholar.org/CorpusID:174811733
16. Pascalau, R., Padurean, V.A., Bartos, D., Bartos, A., Szabo, B.A.: The geometry of the circle of willis anatomical variants as a potential cerebrovascular risk factor. Turk Neurosurg **29**(2), 151–158 (2019)
17. Robben, D., Türetken, E., Sunaert, S., Thijs, V., Wilms, G., Fua, P., Maes, F., Suetens, P.: Simultaneous segmentation and anatomical labeling of the cerebral vasculature. Medical Image Analysis **32**, 201–215 (2016)
18. Shi, Z., Miao, C., Schoepf, U.J., Savage, R.H., Dargis, D.M., Pan, C., Chai, X., Li, X.L., Xia, S., Zhang, X., et al.: A clinically applicable deep-learning model for detecting intracranial aneurysm in computed tomography angiography images. Nature communications **11**(1), 6090 (2020)

19. Szczerba, D., Székely, G.: Macroscopic modeling of vascular systems. In: Dohi, T., Kikinis, R. (eds.) Medical Image Computing and Computer-Assisted Intervention — MICCAI 2002. pp. 284–292. Springer Berlin Heidelberg, Berlin, Heidelberg (2002)
20. Timmins, K., van der Schaaf, I., Bennink, E., et al.: Comparing methods of detecting and segmenting unruptured intracranial aneurysms on TOF-MRAS: The ADAM challenge. NeuroImage **238**, 118216 (2021)
21. Wang, X., Liu, Y., Wu, Z., Mou, X., Zhou, M., Ballester, M.A.G., Zhang, C.: Automatic labeling of vascular structures with topological constraints via hmm. In: Medical Image Computing and Computer-Assisted Intervention- MICCAI 2017: 20th International Conference, Quebec City, QC, Canada, September 11-13, 2017, Proceedings, Part II 20. pp. 208–215. Springer (2017)
22. Zhao, M., Hamarneh, G.: Bifurcation detection in 3d vascular images using novel features and random forest. In: 2014 IEEE 11th International Symposium on Biomedical Imaging (ISBI). pp. 421–424. IEEE (2014)